

Infrared monitoring of OH/IR stars near the Galactic Center

P.R. Wood¹, H.J. Habing², and P.J. McGregor¹

¹ Mount Stromlo and Siding Spring Observatories Private Bag, Weston Creek PO, ACT 2611, Australia

² Sterrewacht Leiden, PO Box 9513, 2300 RA Leiden, The Netherlands

Received 13 February 1998 Accepted 28 April 1998

Abstract. We have monitored 102 fields of size $1' \times 1'$ within $\sim 0.7^\circ$ of the Galactic Center for 1200 days in the K band. Each field was centered on one of the OH/IR stars found by Lindqvist et al. (1992). Infrared colours $J-K$, $H-K$ and $K-L$ were also obtained. Periods have been determined for 80 known OH/IR stars, including 5 from Sjouwerman (1997), and a further 29 previously unknown long-period variables (LPVs) of large (> 0.5 mag.) K amplitude. The overall period distribution of the variables extends from ~ 200 days to ~ 1100 days and it is dominated by LPVs with $P < 600$ days. The existence of LPVs with $P < 300$ days indicates the presence of sub-solar metallicity, old, low mass stars near the Galactic Center. These old LPVs have luminosities equal to those of similar LPVs elsewhere in the Galaxy. However, the LPVs with $P > 300$ days near the Galactic Center have lower luminosities and higher wind expansion velocities v_{exp} at a given period than similar stars in the Galactic bulge or solar vicinity, indicating that the metal abundance of Galactic Center stars is $\sim 2-4$ times solar. Another consequence of the observed low luminosities of the Galactic Center LPVs is that the $(M_{\text{bol}}, \log P)$ and $(K, \log P)$ relations must be metallicity dependent, at least for metallicities of solar or above. The maximum periods and luminosities of Galactic Center LPVs exceed those of bulge LPVs suggesting that there are AGB stars near the Galactic Center which are more massive than any stars in the bulge. AGB masses up to $\sim 4 M_\odot$ are relatively common, with a few AGB stars having masses up to $\sim 7 M_\odot$. There should be ~ 1000 main-sequence precursors in the same volume for each of these massive AGB stars. The high expansion velocity ($v_{\text{exp}} > 18 \text{ km s}^{-1}$) OH/IR stars are separated from the lower expansion velocity OH/IR stars in the $(M_{\text{bol}}, \log P)$ diagram: this separation suggests that the stars with higher v_{exp} have higher metallicity, as well as being younger. The overall results suggest that ongoing star formation and metal enrichment have occurred near the Galactic Center.

Key words: stars: AGB and post-AGB – stars: late-type – stars: oscillations – stars: mass-loss – Galaxy: center

1. Introduction

In the region of the Galaxy near the Galactic Center, there is a mixed stellar population that contains old red giants (Allen 1994) as well as very young stars with masses up to $\sim 100 M_\odot$ (Krabbe et al. 1995; Cotera et al. 1996). These findings lead to the question: is there, near the Center, also a population of intermediate age stars, and has the star formation been a continuous process or, to the contrary, were the stars formed in a few discrete bursts?

One way of detecting intermediate age stars is to look for the very luminous, red, long-period variables (LPVs) that are usually associated with such a population. These stars, which are near the ends of their lives, have very strong stellar winds that produce thick circumstellar envelopes, some of which contain a strong 1612 MHz OH maser. Because the maser is not weakened by interstellar extinction the search for such stars via their radio emission line is highly effective. The first "OH/IR star" was detected in 1975 (Baud et al. 1975) while recent 1612 MHz surveys of the Galactic Center have been made with the VLA by Lindqvist et al. (1992, hereinafter LWHM) and Sjouwerman (1997). These latter surveys consisted of six circular areas of $\sim 30'$ diameter (the VLA primary beam) covering most of the region within $\sim 0.7^\circ$ of the Galactic Center.

In order to get estimates of masses and ages for the OH/IR stars, it is necessary to have measurements of the pulsation period P (typically 400–2000 days) and the bolometric luminosity M_{bol} . Estimates of these quantities for a small number of the brightest of the 134 LWHM sources have been made by Van Langevelde et al. (1993), Jones et al. (1994) and Blommaert et al. (1997). Determination of the properties (masses, luminosities, ages, metal abundances) of the overall population of LPVs near the Galactic Center requires a more extensive survey of the LWHM sources. Such a survey is provided here. In processing our results, we take advantage of the conclusion of the radio observers that there should be a very low number of foreground objects: at most a few of the approximately 150 sources. This allows us to assume that all our objects are at the same distance.

2. Observations and data reduction

The observations were made from March 1994 to June 1997 with the near infrared array camera CASPIR (McGregor et al.

1994) on the 2.3m telescope at Siding Spring Observatory. Each field image was centered on one of the OH/IR stars identified by LWHM. Those fields which had previously been observed in the infrared by Jones et al. (1994) or Blommaert et al. (1997) were not observed. CASPIR pixels of size $0.25''$ were selected, giving an image size of $1' \times 1'$. On any one observing run, first priority was given to obtaining a K image of each field. Once this had been done, any spare time was used for imaging in J , H or L (the L filter used was in fact a narrow band filter centered at $3.59\mu\text{m}$ and of width $0.07\mu\text{m}$). Exposure times of 30 seconds were used for J , H and K and 90 seconds for L .

The images were bias-subtracted, linearized and flat-fielded using the IRAF data reduction package. Photometry of each frame was obtained by running the program DOPHOT (Schechter et al. 1993). For each field, photometry from K frames taken on different dates was matched so that a search could be made for variable stars. When a variable was found associated with an OH/IR star, it appeared within ~ 2 arcseconds of the position given by LWHM, this being the pointing accuracy of the 2.3m telescope. This allowed us to unambiguously rule out the existence of a detectable star in those cases where no signal could be seen at the nominal position of the OH source, and to associate a non-variable but detectable object with a number of OH sources.

As well as the light curves, we also derived $J-K$, $H-K$ and $K-L$ colours for all objects detectable in the relevant filters. However, the colours were derived once only: $J-K$, $H-K$ and $K-L$ were determined, respectively, on Julian dates 2449947, 2449914 and 2450229. Photometric zero points were determined using standard stars in the CASPIR Users Manual (McGregor 1994). Comparison of two separate nights and of standards within each night suggests that the zero points are accurate to 0.03 magnitudes.

3. The search for variables

The matched files of K photometry of each field were searched for variable stars using the phase dispersion minimization (PDM) method of Stellingwerf (1978). Most of the OH/IR stars of LWHM have spectacular light curves that were easily detected. The light curves of these 75 stars are shown in Figs. 1, 2 and 3 along with light curves of 12 non-variable objects that fell at the position expected for the OH source. For an additional 16 sources, no object could be seen (or was only very faintly visible) at the limits of the K frames ($K \sim 14.5$) or the L frame ($L \sim 12$) at the expected position.

In order to derive flux-mean K magnitudes for the variables, some of which have K amplitudes of more than 3 magnitudes, a least-squares Fourier fit (consisting of the fundamental period and first harmonic) was made to each light curve using the period obtained from PDM. The resultant light curve fits are shown as dashed lines on the figures.

The properties of the LWHM OH/IR stars are summarized in Table 1. In this table, Id is the number that LWHM assigned to each of their sources, # is the number of the object within the CASPIR field as given by DOPHOT, $\langle K \rangle$ is the flux-mean K

magnitude derived from the Fourier fit to the light curve, P is the period in days and ΔK is the full amplitude of the K light variations given by the Fourier fit. Note that the $J-K$, $H-K$ and $K-L$ colours are single measurements only. Variations in near-infrared colour with pulsation phase in OH/IR stars have been monitored by Harvey et al. (1974), Engels (1982) and Le Bertre (1993). An examination of this data shows that colour variations increase with pulsation amplitude. For example, $K-L$ variations are small (~ 0.1 mag. full amplitude) for pulsation amplitude $\Delta K \lesssim 1$ mag., increasing to ~ 1 mag. for $\Delta K \sim 3$ mag. The random phase of the colour observation will increase the scatter in colour-magnitude and colour-colour plots but it will be seen that the range of colours is much greater than the colour variation with pulsation phase.

The inner part of the area searched for OH masers by LWHM has recently been re-examined by Sjouwerman (1997) who has detected many more fainter OH sources. Ten of these new sources fell within the CASPIR fields centered on the LWHM sources and 5 were detected. The K light curves of these stars are shown in Fig. 4 and their properties are summarized in Table 2. Id and # are, respectively, the LWHM number of the CASPIR field and the DOPHOT number in the field while Name is the identification given by Sjouwerman (1997).

In addition to the previously known OH maser sources, many objects in the fields studied showed variability. Most objects were semi-regular or irregular variables of small amplitude ($\Delta K < 0.5$ mag.), some objects showing monotonic rises or declines over the 1200 days of observation. Other objects showed a clear periodic variation. There were 29 such objects with amplitude greater than 0.5 mag. and their light curves are shown in Fig. 5. Their properties are summarized in Table 3. The coordinates for each variable were computed as offsets from the positions of the LWHM source in each frame (when detected) and should be as accurate as the LWHM positions (when the LWHM source was not detected, positional errors up to $3''$ are possible).

Finally, we make some comments on the LWHM sources which do not appear to vary in Figs. 1, 2 and 3. Sources 4, 31, 59 and 69 are relatively blue, consistent with them being normal giants spatially coincident with the OH/IR star. The magnitudes given for these stars are probably not those of the OH/IR star. Source 68 is a close double which clearly varies at L , but a period could not be determined from the K magnitude, which is dominated by the companion. Sources 63 and 70 are clearly variable at L but no period could be determined from the K photometry. There remain 4 sources, numbers 60, 90, 107 and 122 which are red and visible at K and L but which showed no evidence for variability. It is possible that these are post-AGB stars. We also note that there are 16 sources which were not detected at K and for which there is therefore no variability information (see the list at the end of Table 1). These sources are also potential post-AGB stars.

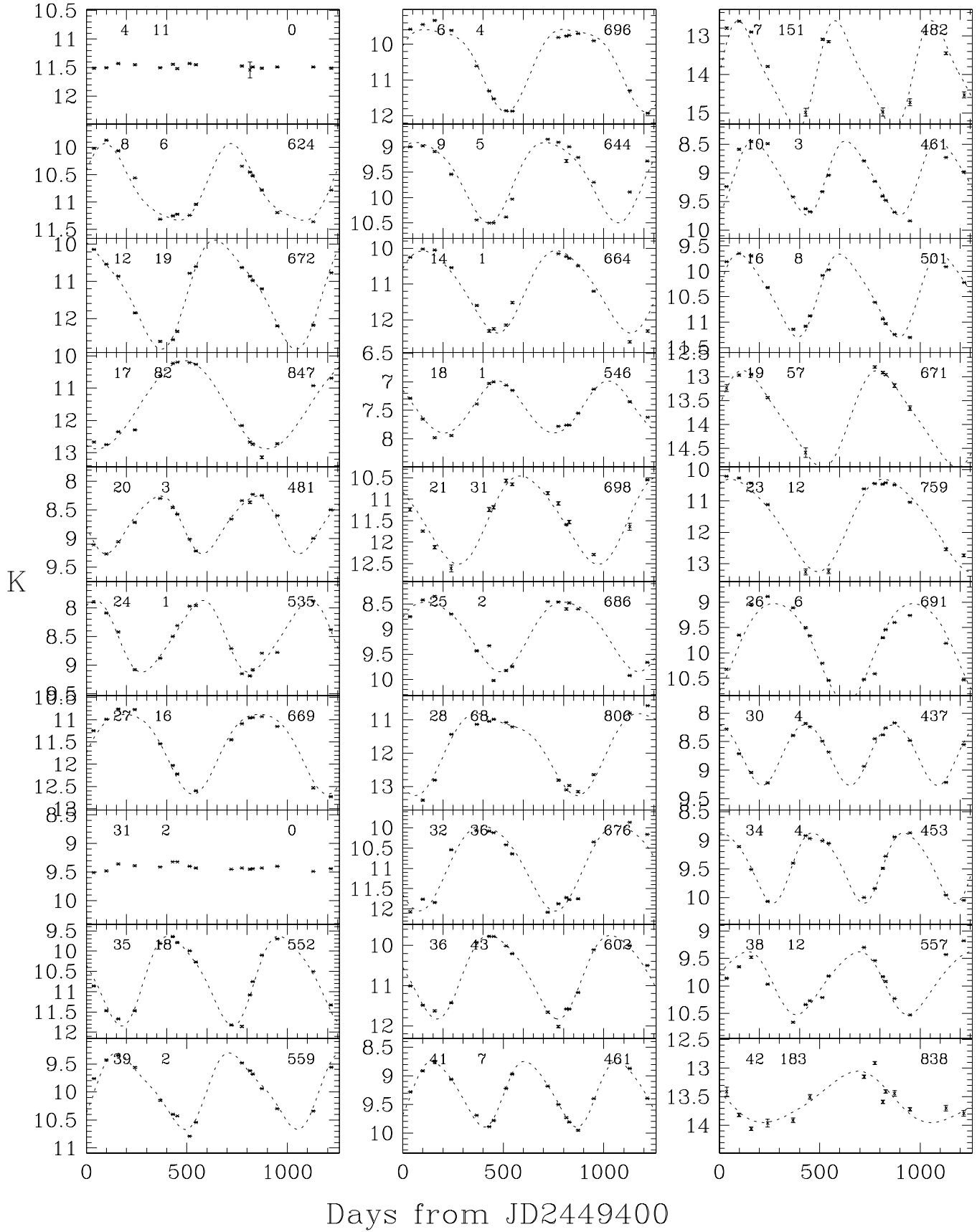


Fig. 1. *K* light curves of the first 30 detected LWHM sources. Each point has an error bar as given by the photometry package DOPHOT. The dashed curve is the Fourier fit to the light curve described in the text. The three numbers of each figure are, from left to right, the LWHM field Id, the DOPHOT number # and the period in days as given in Table 1.

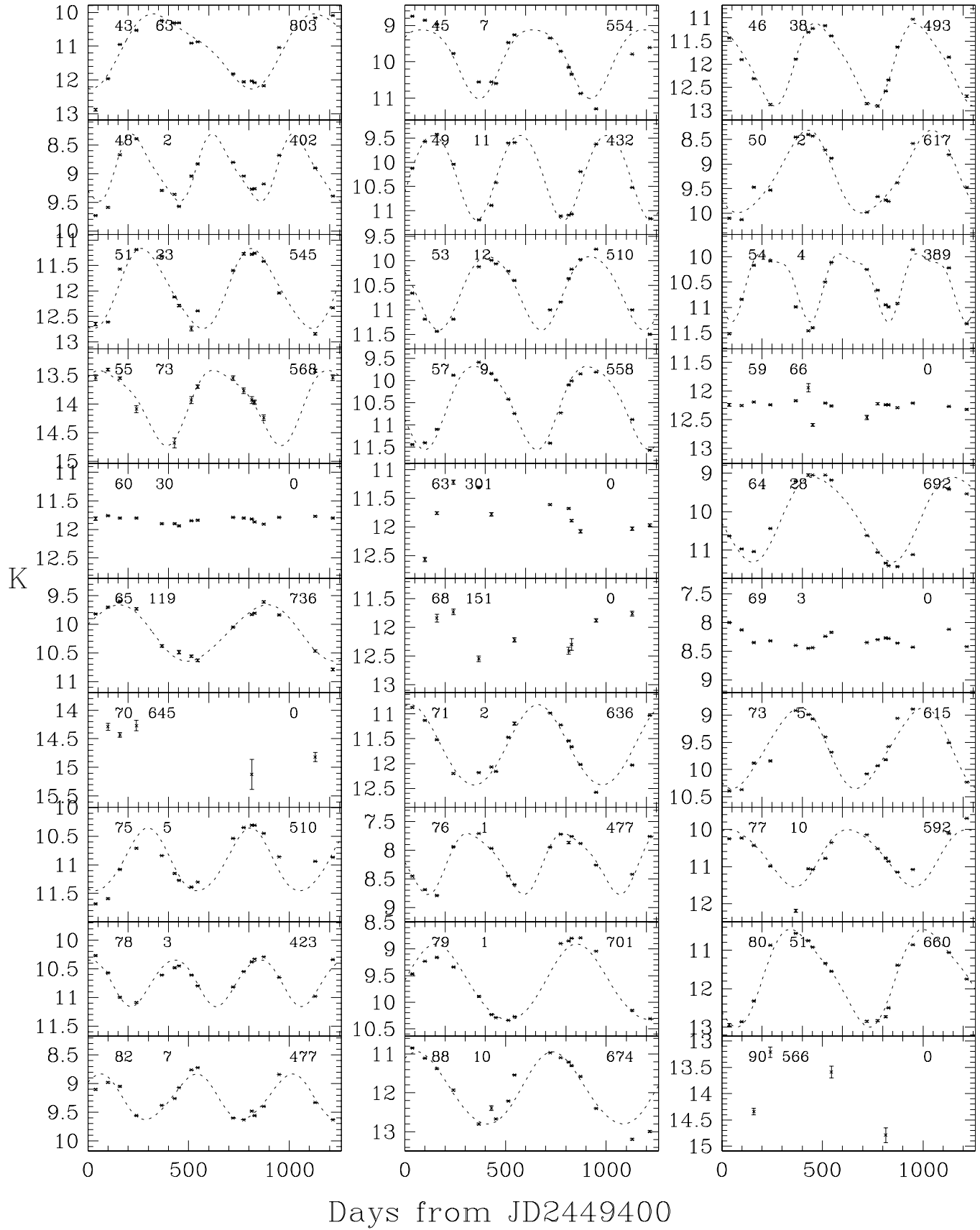


Fig. 2. Same as Fig. 1 but for the second 30 detected LWHM sources.

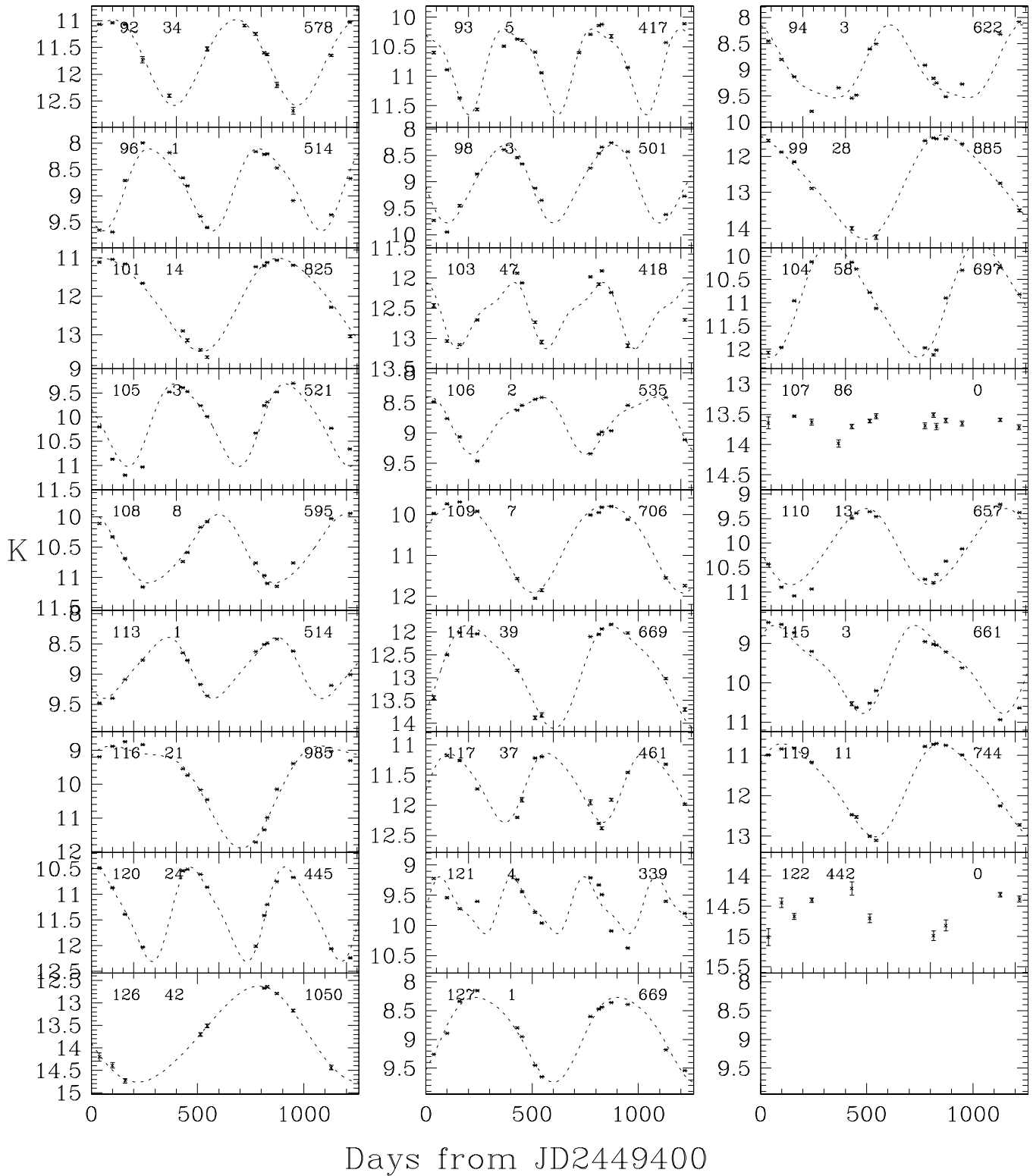


Fig. 3. Same as Fig. 1 but for the final 26 detected LWHM sources.

4. Reddening and the $(H - K, K - L)$ and $(K, K - L)$ diagrams

The OH/IR stars are shown in the $(H - K, K - L)$ plane in Fig. 6 together with all the isolated, non-variable stars obtained from

the photometry of the images. Also shown in Fig. 6 are the position of unreddened, non-variable red giants in the Baade’s window (Frogel & Whitford 1987) and the position of the LPVs in Baade’s Window (including IRAS sources) from Glass et al.

Table 1. Properties of LWHM OH/IR stars

| Id | # | $\langle K \rangle$ | $J-K$ | $H-K$ | $K-L$ | P | ΔK | Id | # | $\langle K \rangle$ | $J-K$ | $H-K$ | $K-L$ | P | ΔK |
|----|-----|---------------------|-------|-------|-------|-----|------------|-----|-----|---------------------|-------|-------|-------|------|------------|
| 4 | 11 | 11.48 | - | 2.12 | 1.58 | - | - | 63 | 301 | 11.66 | - | - | 3.97 | - | - |
| 6 | 4 | 10.22 | - | - | 3.84 | 696 | 2.31 | 64 | 28 | 9.87 | - | 3.22 | 4.04 | 692 | 2.21 |
| 7 | 151 | 13.65 | - | - | 5.90 | 482 | 2.80 | 65 | 119 | 10.10 | - | 3.38 | 3.77 | 736 | 0.99 |
| 8 | 6 | 10.63 | - | - | 3.13 | 624 | 1.40 | 68 | 34 | 11.24 | - | 2.39 | 1.46 | - | - |
| 9 | 5 | 9.46 | - | 3.30 | 3.00 | 644 | 1.58 | 69 | 3 | 8.30 | 6.60 | 2.01 | 1.42 | - | - |
| 10 | 3 | 8.98 | 6.17 | 2.56 | 2.20 | 461 | 1.30 | 70 | 645 | 14.79 | - | - | 5.23 | - | - |
| 12 | 19 | 10.85 | - | - | 3.96 | 672 | 2.94 | 71 | 2 | 11.50 | - | - | 4.38 | 636 | 1.62 |
| 14 | 1 | 10.87 | - | - | 3.71 | 664 | 2.30 | 73 | 5 | 9.48 | - | 3.16 | 3.39 | 615 | 1.48 |
| 16 | 8 | 10.30 | - | 3.44 | 3.50 | 501 | 1.64 | 75 | 5 | 10.88 | - | - | 2.17 | 510 | 1.10 |
| 17 | 82 | 11.11 | - | 3.69 | 4.86 | 847 | 2.73 | 76 | 1 | 8.13 | 5.73 | 2.18 | 2.08 | 477 | 1.06 |
| 18 | 1 | 7.41 | 4.62 | 1.70 | 1.97 | 546 | 0.91 | 77 | 10 | 10.59 | - | 3.96 | 3.55 | 592 | 1.55 |
| 19 | 57 | 13.67 | - | - | 3.87 | 671 | 2.03 | 78 | 3 | 10.69 | - | 3.98 | 3.04 | 423 | 0.81 |
| 20 | 3 | 8.67 | 6.86 | 2.40 | 2.13 | 481 | 1.01 | 79 | 1 | 9.55 | 6.09 | 2.88 | 3.29 | 701 | 1.42 |
| 21 | 31 | 11.21 | - | - | 4.52 | 698 | 2.05 | 80 | 51 | 11.34 | - | 3.88 | 4.51 | 660 | 2.54 |
| 23 | 12 | 11.25 | - | - | 4.36 | 759 | 2.95 | 82 | 7 | 9.21 | 7.01 | 2.56 | 2.69 | 477 | 0.80 |
| 24 | 1 | 8.42 | 5.84 | 2.12 | 2.45 | 535 | 1.26 | 88 | 10 | 11.72 | - | - | 4.36 | 674 | 1.85 |
| 25 | 2 | 8.97 | - | 3.28 | 2.78 | 686 | 1.38 | 90 | 566 | 14.15 | - | - | 6.39 | - | - |
| 26 | 6 | 9.68 | - | 3.30 | 3.39 | 691 | 1.94 | 92 | 34 | 11.59 | - | - | 3.96 | 578 | 1.59 |
| 27 | 16 | 11.46 | - | - | 3.70 | 669 | 1.79 | 93 | 5 | 10.69 | 5.34 | 2.39 | 3.21 | 417 | 1.45 |
| 28 | 68 | 11.54 | - | 4.08 | 5.42 | 806 | 2.47 | 94 | 3 | 8.85 | - | 2.93 | 2.82 | 622 | 1.40 |
| 30 | 4 | 8.64 | 5.30 | 1.88 | 1.93 | 437 | 1.06 | 96 | 1 | 8.69 | - | 2.78 | 2.68 | 514 | 1.57 |
| 31 | 2 | 9.43 | 5.49 | 1.85 | 1.44 | - | - | 98 | 3 | 8.88 | - | 2.57 | 2.42 | 501 | 1.49 |
| 32 | 36 | 10.66 | - | 3.68 | 4.59 | 676 | 2.09 | 99 | 28 | 12.39 | - | - | 5.12 | 885 | 2.89 |
| 34 | 4 | 9.35 | 6.29 | 2.36 | 2.76 | 453 | 1.23 | 101 | 14 | 11.85 | - | - | 4.77 | 825 | 2.43 |
| 35 | 18 | 10.40 | - | 3.60 | 4.11 | 552 | 2.22 | 103 | 47 | 12.52 | - | 2.75 | 4.01 | 418 | 1.10 |
| 36 | 43 | 10.48 | - | 3.25 | 4.08 | 602 | 2.08 | 104 | 58 | 10.63 | - | 2.88 | 4.29 | 697 | 2.48 |
| 38 | 12 | 9.85 | - | 3.61 | 2.84 | 557 | 1.15 | 105 | 3 | 9.95 | - | 3.34 | 3.44 | 521 | 1.71 |
| 39 | 2 | 9.87 | - | 3.80 | 3.17 | 559 | 1.37 | 106 | 2 | 8.76 | 6.68 | 2.33 | 2.16 | 535 | 0.94 |
| 41 | 7 | 9.22 | - | 2.86 | 2.64 | 461 | 1.15 | 107 | 86 | 13.62 | - | - | 3.60 | - | - |
| 42 | 183 | 13.48 | - | - | 5.95 | 838 | 0.90 | 108 | 8 | 10.49 | - | - | 3.28 | 595 | 1.13 |
| 43 | 63 | 10.84 | - | 4.16 | 4.50 | 803 | 2.22 | 109 | 7 | 10.48 | - | - | 3.61 | 706 | 2.13 |
| 45 | 7 | 9.71 | - | 3.22 | 3.00 | 554 | 1.89 | 110 | 13 | 9.94 | - | 3.16 | 3.43 | 657 | 1.56 |
| 46 | 38 | 11.80 | - | 3.95 | 4.46 | 493 | 1.78 | 113 | 1 | 8.84 | - | 2.78 | 2.22 | 514 | 1.01 |
| 48 | 2 | 8.84 | 5.78 | 2.23 | 2.18 | 402 | 1.18 | 114 | 39 | 12.62 | - | - | 4.45 | 669 | 2.26 |
| 49 | 11 | 10.09 | 6.69 | 2.88 | 3.55 | 432 | 1.75 | 115 | 3 | 9.36 | - | 4.07 | 3.02 | 661 | 2.24 |
| 50 | 2 | 9.06 | 7.48 | 2.73 | 3.27 | 617 | 1.68 | 116 | 21 | 9.62 | - | - | 4.66 | 985 | 3.03 |
| 51 | 23 | 11.84 | - | - | 3.95 | 545 | 1.57 | 117 | 37 | 11.60 | - | 3.23 | 3.92 | 461 | 1.15 |
| 53 | 12 | 10.47 | - | 3.91 | 2.99 | 510 | 1.51 | 119 | 11 | 11.52 | - | - | 4.45 | 744 | 2.31 |
| 54 | 4 | 10.38 | - | 3.52 | 3.32 | 389 | 1.35 | 120 | 24 | 11.18 | - | 3.79 | 3.00 | 445 | 1.85 |
| 55 | 73 | 13.90 | - | - | 5.01 | 568 | 1.31 | 121 | 4 | 9.65 | - | 2.82 | 0.96 | 339 | 0.94 |
| 57 | 9 | 10.31 | - | 3.47 | 3.24 | 558 | 1.88 | 122 | 442 | 14.59 | - | - | - | - | - |
| 59 | 66 | 12.31 | - | 1.76 | - | - | - | 126 | 42 | 13.47 | - | - | 6.05 | 1050 | 2.14 |
| 60 | 30 | 11.87 | - | - | 2.59 | - | - | 127 | 1 | 8.80 | - | 3.19 | 2.83 | 669 | 1.48 |

No objects were seen in K or L at the positions of LWHM sources 1, 2, 3, 11, 13, 61, 62, 66, 72, 74, 89, 102, 123 or 124. LWHM sources 15 and 56 were detected at L and had $L = 11.6$ and 9.62 , respectively, on JD2450229.

(1995) and Wood & Bessell (1983). The arrow shows a reddening vector corresponding to 30 magnitudes of visual extinction (see below for the reddening law used).

It is clear from Fig. 6 that the vast majority of objects seen in the infrared are highly reddened with $A_V \sim 12$ to 30 magnitudes. An examination of individual ($1' \times 1'$) fields showed that the reddening varied distinctly between fields. A median $E(H-K)$ was derived for each field as follows. Firstly, the median $H-K$ of all isolated stars with $K < 14$ and $H-K >$

0.7 was computed for each field (stars with $H-K < 0.7$ are clearly foreground objects). The extinction was derived from $H-K$ rather than $K-L$ because of the large number of stars detected in both H and K . It was then assumed that the majority of the stars detected in each field were red giants with intrinsic $H-K=0.25$. The difference between the median $H-K$ and 0.25 gave the median $E(H-K)$ for each field.

The points shown in Fig. 6 were dereddened using the following procedure. From Fig. 6 we find that in our photometric

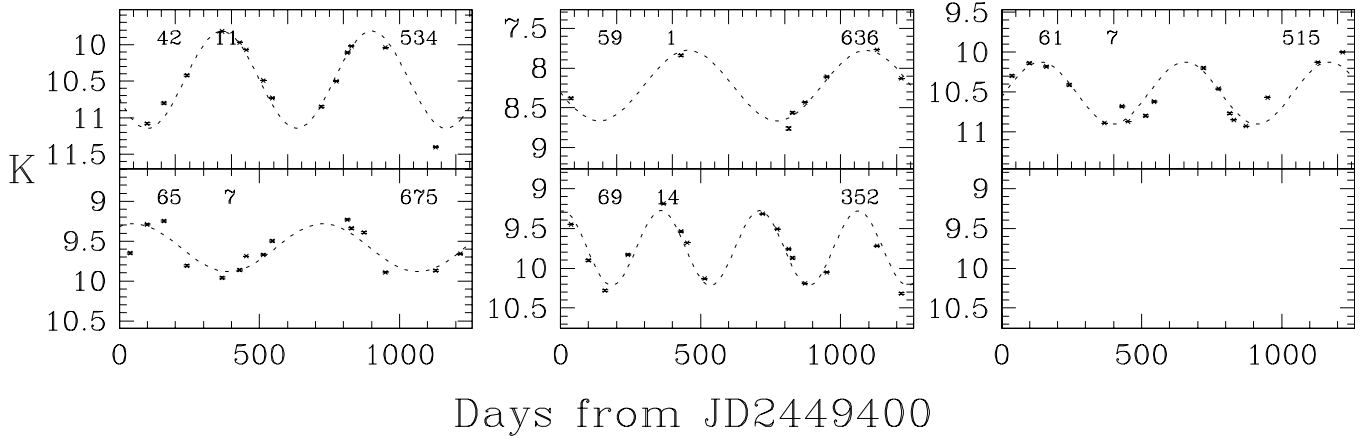


Fig. 4. Same as Fig. 1 but for the Sjouwerman sources.

Table 2. Properties of Sjouwerman (1997) OH/IR stars

| Id | # | Name | $\langle K \rangle$ | $J-K$ | $H-K$ | $K-L$ | P | ΔK |
|----|----|---------------|---------------------|-------|-------|-------|-----|------------|
| 42 | 11 | 359.797-0.025 | 10.38 | - | 2.98 | 3.32 | 534 | 1.33 |
| 59 | 1 | 359.918-0.055 | 8.18 | - | - | - | 636 | 0.88 |
| 61 | 7 | 359.932-0.059 | 10.48 | - | 3.27 | 1.67 | 515 | 0.78 |
| 65 | 7 | 359.947-0.046 | 9.56 | 6.75 | 2.00 | 1.90 | 675 | 0.60 |
| 69 | 14 | 359.965-0.043 | 9.70 | - | 2.45 | 2.14 | 352 | 0.94 |

No objects were seen at the positions of the Sjouwerman sources 359.931-0.050, 359.943-0.055, 359.956-0.050, 359.970-0.047, 359.934-0.059 and 359.972-0.046.

system $E(K-L) = 0.72 E(H-K)$. This relation was used to calculate a median $E(K-L)$ for each field from the $E(H-K)$ derived above. Then we used the relation $A_K = 2.07 E(K-L)$ from Rieke & Lebofsky (1985) to calculate the extinction. The dereddened points are shown replotted in Fig. 7. The scatter of the non-variable stars along the reddening vector is now greatly reduced although a residual scatter in reddening exists due to reddening variations on spatial scales less than one arcminute.

The OH/IR stars are well separated from the non-variable stars in Fig. 7. The majority of the OH/IR stars discovered by LWHM lie beyond the sequence occupied by the LPVs in the Baade’s Window while the Sjouwerman sources and the newly-discovered variables mostly lie near the bulge LPV sequence. Those LWHM variables lying beyond the bulge sequence presumably have thicker and/or cooler circumstellar shells than the variables (including IRAS sources) in Baade’s window. However, very red objects similar to the LWHM sources are known to exist in the direction of the bulge - about a dozen of them were found by Whitelock et al. (1991) who monitored IRAS sources in a 60 deg^2 area of the bulge between $|b| = 7^\circ$ to 8° . Massive, variable OH/IR stars which are even redder are known to occur along the Galactic plane (eg. Engels et al. 1983)

A similar separation of the non-variable stars and the variable stars is seen in the $(K, K-L)$ diagram, Fig. 8. The non-variable red giant branch occurs in the position expected for a Baade’s window giant branch reddened by $\sim 20-25 \text{ mag.}$ of visual extinction. Once again, the large circumstellar reddening

and/or cool shells of the OH sources of LWHM is apparent. The Sjouwerman OH sources and the newly discovered variables are mostly less extreme in their $K-L$ colours than the OH/IR stars discovered by LWHM and they bridge the gap between the non-variable and the OH/IR sequences.

5. Bolometric magnitudes

Bolometric luminosities were calculated by applying a bolometric correction BC_L to L_0 , the extinction-corrected L . The reddenings derived above were used to compute L_0 . In order to estimate BC_L , we selected from the literature various LPVs and IRAS sources towards the Galactic bulge for which infrared photometry existed and for which bolometric magnitudes had been derived by integrating under the observed flux distribution. For $K-L < 1$, the data of Wood & Bessell (1983) were used. For stars with redder intrinsic colours (i.e. substantial circumstellar shells), the IRAS sources with periods $P > 500$ days listed in Table 3 of Whitelock et al. (1991) were used. Note that the interstellar extinction to all these objects is relatively small compared to the extinction to the Galactic Center OH/IR stars, while their intrinsic colour range matches that of the OH/IR stars.

The data of Wood & Bessell and of Whitelock et al. used L and BC_L defined at 3.8 and $3.45 \mu\text{m}$, respectively. The conversion of $K-[3.8]$ to $K-[3.45]$ for very red stars was obtained by using the data in Table 2a of Blommaert et al. (1993): a

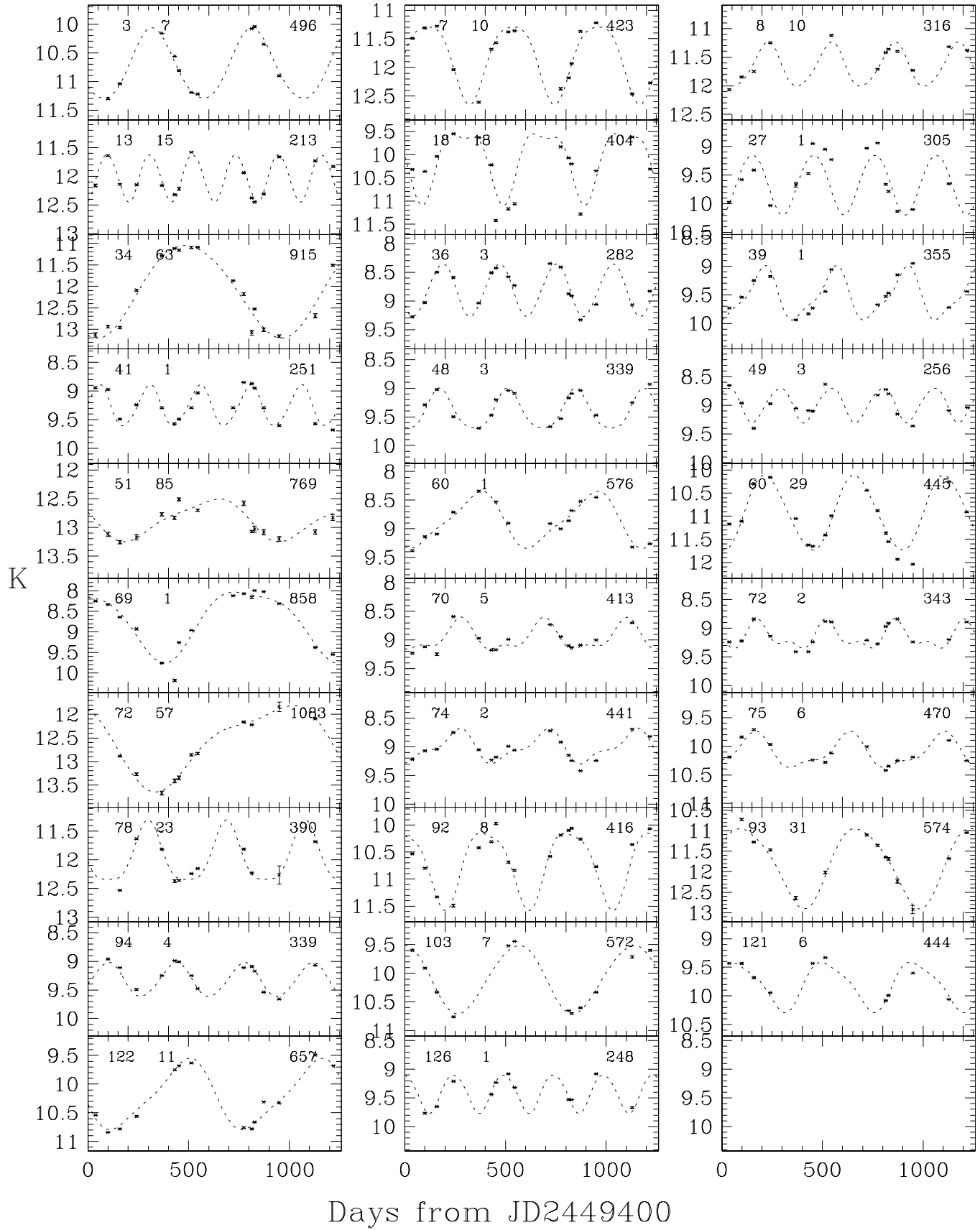


Fig. 5. Same as Fig. 1 but for periodic variables identified in this study.

Table 3. New periodic variable stars

| Id | # | RA(1950) | Dec(1950) | $\langle K \rangle$ | $J-K$ | $H-K$ | $K-L$ | P | ΔK |
|-----|----|------------|-----------|---------------------|-------|-------|-------|------|------------|
| 3 | 7 | 17 40 56.2 | -29 23 30 | 10.63 | - | 3.98 | - | 496 | 1.23 |
| 7 | 10 | 17 41 22.6 | -29 21 51 | 11.74 | - | 4.61 | 3.53 | 423 | 1.35 |
| 8 | 10 | 17 41 26.0 | -29 21 50 | 11.62 | - | - | 1.40 | 316 | 0.78 |
| 13 | 15 | 17 42 20.4 | -29 23 49 | 11.99 | - | - | 2.85 | 213 | 0.83 |
| 18 | 18 | 17 41 55.2 | -29 15 53 | 9.98 | - | 2.68 | 2.60 | 404 | 1.55 |
| 27 | 1 | 17 41 40.3 | -29 8 7 | 9.59 | - | - | 1.60 | 305 | 1.04 |
| 34 | 63 | 17 42 3.5 | -29 8 7 | 11.81 | - | 4.00 | 3.89 | 915 | 2.16 |
| 36 | 3 | 17 42 42.1 | -29 13 31 | 8.76 | 4.38 | 1.47 | 1.47 | 282 | 0.92 |
| 39 | 1 | 17 43 26.4 | -29 18 23 | 9.46 | 6.78 | 2.39 | 2.11 | 355 | 0.95 |
| 41 | 1 | 17 41 20.6 | -28 59 47 | 9.24 | 4.72 | 1.42 | 1.41 | 251 | 0.72 |
| 48 | 3 | 17 41 57.3 | -29 2 29 | 9.38 | 6.69 | 2.27 | 1.80 | 339 | 0.70 |
| 49 | 3 | 17 44 8.0 | -29 19 29 | 8.96 | - | 1.59 | 1.47 | 256 | 0.61 |
| 51 | 85 | 17 42 55.4 | -29 8 22 | 12.82 | - | - | - | 769 | 0.75 |
| 60 | 1 | 17 42 7.9 | -28 57 29 | 8.80 | - | 2.81 | 2.33 | 576 | 1.00 |
| 60 | 29 | 17 42 8.5 | -28 57 48 | 10.79 | - | 3.43 | 3.04 | 445 | 1.62 |
| 69 | 1 | 17 42 32.1 | -28 57 52 | 8.57 | - | 2.77 | 2.47 | 858 | 1.73 |
| 70 | 5 | 17 42 48.1 | -29 0 4 | 8.94 | - | 2.23 | 1.74 | 413 | 0.56 |
| 72 | 2 | 17 42 44.0 | -28 58 45 | 9.14 | 5.66 | 1.90 | 1.74 | 343 | 0.52 |
| 72 | 57 | 17 42 42.6 | -28 59 26 | 12.44 | - | - | - | 1083 | 1.83 |
| 74 | 2 | 17 42 59.5 | -28 59 35 | 8.99 | - | 2.51 | 1.98 | 441 | 0.62 |
| 75 | 6 | 17 42 42.8 | -28 57 4 | 10.09 | - | - | 1.70 | 470 | 0.63 |
| 78 | 23 | 17 41 51.8 | -28 49 45 | 11.88 | - | - | - | 390 | 1.04 |
| 92 | 8 | 17 42 51.2 | -28 48 51 | 10.62 | 5.19 | 2.38 | 3.01 | 416 | 1.44 |
| 93 | 31 | 17 42 49.8 | -28 49 5 | 11.64 | - | - | 4.20 | 574 | 1.96 |
| 94 | 4 | 17 43 17.4 | -28 52 31 | 9.31 | - | 2.17 | 1.80 | 339 | 0.59 |
| 103 | 7 | 17 42 54.5 | -28 42 51 | 10.01 | - | 3.52 | 3.26 | 572 | 1.20 |
| 121 | 6 | 17 43 21.3 | -28 30 1 | 9.77 | - | 2.20 | 1.65 | 444 | 0.88 |
| 122 | 11 | 17 43 27.3 | -28 31 19 | 10.12 | - | 4.00 | 2.14 | 657 | 1.25 |
| 126 | 1 | 17 44 29.8 | -28 34 21 | 9.39 | - | 1.72 | 1.45 | 248 | 0.67 |

good fit to the data is $K-[3.8] = 1.12(K-[3.45])$. For our L filter defined at $3.59 \mu\text{m}$, we interpolate to derive $K-[3.59] = 1.05(K-[3.45])$. Similarly, we made an appropriate modification to the bolometric corrections. For example, by definition, $m_{\text{bol}} = [3.45] + BC_{3.45} = [3.59] + BC_{3.59}$ so that $BC_{3.59} = BC_{3.45} + (K-[3.59]) - (K-[3.45]) = BC_{3.45} + 0.05(K-[3.45])$. In Fig. 9, we plot BC_L against $K-L$ (where L is defined at $3.59 \mu\text{m}$). Also shown on the figure is the BC_L of Blommaert et al. (1997) (converted to our L filter) and a fitting function that we have used to derive BC_L from $K-L$. There is clearly a large scatter in the individual BC_L values. Our fitting function agrees with that of Blommaert et al. (1997) to within 0.2 magnitudes for $K-L < 3.6$, which is where the majority of our objects lie. An examination of modelling of the spectral energy distributions of oxygen-rich stars with thick envelopes by Le Sidaner and Le Bertre (1993, 1996), combined with the measurements by Le Bertre (1993), confirms the results of Fig. 9. For stars with very thick envelopes ($K-L > 5$) these model spectra predict a larger BC_L than we use here, as do the results of Blommaert et al. (1997). However, only two of our objects are this red.

Given the reddening, the observed K and L magnitudes, and BC_L , the apparent bolometric magnitude m_{bol} can be derived for each source. The reddening $E(H-K)$, dereddened K magnitude K_0 , intrinsic colour $(K-L)_0$, m_{bol} and the period

are given in Tables 4, 5 and 6 for the LWHM sources, the Sjouwerman(1997) sources, and the new variables, respectively.

6. The $(M_K, \log P)$ and $(M_{\text{bol}}, \log P)$ relations

The $(M_K, \log P)$ and $(M_{\text{bol}}, \log P)$ relations for the Galactic Center variables are shown in Figs. 10 and 11, respectively. LPVs in the Baade's Window field of Glass et al. (1995) are also shown along with LMC OH/IR stars from Wood et al. (1992) and a line representing the position of optically visible LPVs in the LMC from Hughes & Wood (1990) (see also Feast et al. 1989). The LMC line is split into two parts, the shorter period end representing the LMC LPVs with masses $\lesssim 1.5 M_\odot$ while the longer period part of the line represents more massive LPVs with $1.5 \lesssim M/M_\odot \lesssim 6$. Distances of 8.9 kpc to the Galactic Center, 8.7 kpc to the Baade's Window field and 51.3 kpc (distance modulus 18.55) to the LMC have been used for consistency with the results of Glass et al. (1995).

It is clear that the majority of the Galactic Center objects do not follow the LMC $(M_K, \log P)$ relation for optically visible LPVs and nearly all lie well below it, with offsets of up to 6 magnitudes. This indicates that most of these objects are surrounded by cool, dense, dusty shells that obscure the central stars in K . On the other hand, the majority of the Baade's Window LPVs lie on the LMC $(M_K, \log P)$ relation as expected

Table 4. Reddening and intrinsic properties of LWHM sources

| LWHM | # | $E(H-K)$ | $\langle K_0 \rangle$ | $(K-L)_0$ | m_{bol} | P | LWHM | # | $E(H-K)$ | $\langle K_0 \rangle$ | $(K-L)_0$ | m_{bol} | P |
|------|-----|----------|-----------------------|-----------|------------------|-----|------|-----|----------|-----------------------|-----------|------------------|------|
| 4 | 11 | 1.85 | 8.72 | 0.25 | 11.14 | - | 63 | 301 | 1.93 | 8.78 | 2.58 | 10.36 | - |
| 6 | 4 | 1.45 | 8.06 | 2.80 | 9.32 | 696 | 64 | 28 | 0.97 | 8.42 | 3.34 | 8.82 | 692 |
| 7 | 151 | 2.05 | 10.60 | 4.43 | 9.10 | 482 | 65 | 119 | 1.52 | 7.83 | 2.68 | 9.27 | 736 |
| 8 | 6 | 1.67 | 8.14 | 1.93 | 10.57 | 624 | 68 | 34 | 1.86 | 8.47 | 0.12 | 10.29 | - |
| 9 | 5 | 1.22 | 7.64 | 2.12 | 9.84 | 644 | 69 | 3 | 1.53 | 6.02 | 0.32 | 8.64 | - |
| 10 | 3 | 1.35 | 6.97 | 1.23 | 10.02 | 461 | 70 | 645 | 1.69 | 12.27 | 4.01 | 11.52 | - |
| 12 | 19 | 1.62 | 8.44 | 2.80 | 9.70 | 672 | 71 | 2 | 1.42 | 9.38 | 3.36 | 9.76 | 636 |
| 14 | 1 | 1.41 | 8.77 | 2.70 | 10.18 | 664 | 73 | 5 | 1.40 | 7.39 | 2.38 | 9.25 | 615 |
| 16 | 8 | 1.45 | 8.14 | 2.46 | 9.90 | 501 | 75 | 5 | 1.43 | 8.75 | 1.14 | 11.85 | 510 |
| 17 | 82 | 1.44 | 8.96 | 3.82 | 8.54 | 847 | 76 | 1 | 1.11 | 6.48 | 1.28 | 9.50 | 477 |
| 18 | 1 | 1.38 | 5.35 | 0.98 | 8.50 | 546 | 77 | 10 | 1.78 | 7.94 | 2.27 | 9.95 | 592 |
| 19 | 57 | 1.20 | 11.88 | 3.01 | 12.82 | 671 | 78 | 3 | 1.95 | 7.78 | 1.64 | 10.52 | 423 |
| 20 | 3 | 1.39 | 6.60 | 1.13 | 9.70 | 481 | 79 | 1 | 1.05 | 7.99 | 2.54 | 9.63 | 701 |
| 21 | 31 | 1.30 | 9.27 | 3.59 | 9.26 | 698 | 80 | 51 | 1.60 | 8.96 | 3.36 | 9.33 | 660 |
| 23 | 12 | 1.49 | 9.03 | 3.29 | 9.52 | 759 | 82 | 7 | 1.50 | 6.98 | 1.61 | 9.74 | 477 |
| 24 | 1 | 1.34 | 6.42 | 1.49 | 9.30 | 535 | 88 | 10 | 2.28 | 8.32 | 2.72 | 9.70 | 674 |
| 25 | 2 | 1.61 | 6.57 | 1.62 | 9.33 | 686 | 90 | 566 | 1.38 | 12.09 | 5.40 | 8.78 | - |
| 26 | 6 | 1.64 | 7.24 | 2.21 | 9.32 | 691 | 92 | 34 | 1.42 | 9.47 | 2.94 | 10.52 | 578 |
| 27 | 16 | 1.57 | 9.12 | 2.57 | 10.72 | 669 | 93 | 5 | 1.44 | 8.54 | 2.17 | 10.68 | 417 |
| 28 | 68 | 1.18 | 9.78 | 4.57 | 8.02 | 806 | 94 | 3 | 1.59 | 6.48 | 1.68 | 9.18 | 622 |
| 30 | 4 | 1.08 | 7.03 | 1.15 | 10.12 | 437 | 96 | 1 | 1.00 | 7.20 | 1.96 | 9.60 | 514 |
| 31 | 2 | 1.22 | 7.61 | 0.56 | 10.63 | - | 98 | 3 | 1.34 | 6.88 | 1.46 | 9.78 | 501 |
| 32 | 36 | 1.38 | 8.60 | 3.60 | 8.57 | 676 | 99 | 28 | 1.25 | 10.53 | 4.22 | 9.40 | 885 |
| 34 | 4 | 1.48 | 7.14 | 1.70 | 9.83 | 453 | 101 | 14 | 1.02 | 10.33 | 4.04 | 9.54 | 825 |
| 35 | 18 | 1.08 | 8.79 | 3.33 | 9.20 | 552 | 103 | 47 | 1.56 | 10.20 | 2.89 | 11.32 | 418 |
| 36 | 43 | 1.15 | 8.77 | 3.25 | 9.31 | 602 | 104 | 58 | 1.00 | 9.14 | 3.57 | 9.16 | 697 |
| 38 | 12 | 1.61 | 7.45 | 1.68 | 10.15 | 557 | 105 | 3 | 1.51 | 7.70 | 2.35 | 9.60 | 521 |
| 39 | 2 | 1.57 | 7.53 | 2.04 | 9.83 | 559 | 106 | 2 | 1.49 | 6.54 | 1.09 | 9.66 | 535 |
| 41 | 7 | 1.33 | 7.24 | 1.68 | 9.93 | 461 | 107 | 86 | 1.50 | 11.38 | 2.52 | 13.05 | - |
| 42 | 183 | 1.49 | 11.26 | 4.88 | 8.93 | 838 | 108 | 8 | 1.78 | 7.84 | 2.00 | 10.19 | 595 |
| 43 | 63 | 1.00 | 9.35 | 3.78 | 9.01 | 803 | 109 | 7 | 1.00 | 8.99 | 2.89 | 10.11 | 706 |
| 45 | 7 | 1.64 | 7.27 | 1.82 | 9.82 | 554 | 110 | 13 | 1.22 | 8.12 | 2.55 | 9.74 | 657 |
| 46 | 38 | 1.31 | 9.85 | 3.52 | 9.95 | 493 | 113 | 1 | 1.53 | 6.56 | 1.12 | 9.67 | 514 |
| 48 | 2 | 1.36 | 6.81 | 1.20 | 9.88 | 402 | 114 | 39 | 1.22 | 10.80 | 3.57 | 10.81 | 669 |
| 49 | 11 | 1.21 | 8.29 | 2.68 | 9.72 | 432 | 115 | 3 | 0.99 | 7.88 | 2.31 | 9.85 | 661 |
| 50 | 2 | 1.14 | 7.36 | 2.45 | 9.13 | 617 | 116 | 21 | 1.06 | 8.04 | 3.90 | 7.49 | 985 |
| 51 | 23 | 1.38 | 9.78 | 2.96 | 10.80 | 545 | 117 | 37 | 1.16 | 9.87 | 3.09 | 10.69 | 461 |
| 53 | 12 | 1.85 | 7.71 | 1.66 | 10.43 | 510 | 119 | 11 | 1.53 | 9.24 | 3.35 | 9.63 | 744 |
| 54 | 4 | 1.20 | 8.59 | 2.46 | 10.35 | 389 | 120 | 24 | 1.48 | 8.97 | 1.94 | 11.40 | 445 |
| 55 | 73 | 1.78 | 11.25 | 3.73 | 10.99 | 568 | 121 | 4 | 1.14 | 7.95 | 0.14 | 9.88 | 339 |
| 57 | 9 | 1.54 | 8.02 | 2.13 | 10.20 | 558 | 122 | 442 | 1.11 | 12.94 | - | - | - |
| 59 | 66 | 1.89 | 9.49 | - | - | - | 126 | 42 | 1.32 | 11.50 | 5.10 | 8.75 | 1050 |
| 60 | 30 | 1.79 | 9.20 | 1.30 | 12.21 | - | 127 | 1 | 1.62 | 6.39 | 1.67 | 9.10 | 669 |

Table 5. Reddening and intrinsic properties of Sjouwerman sources

| LWHM | # | $E(H-K)$ | $\langle K_0 \rangle$ | $(K-L)_0$ | m_{bol} | P |
|------|----|----------|-----------------------|-----------|------------------|-----|
| 42 | 11 | 1.49 | 8.16 | 2.25 | 10.20 | 534 |
| 59 | 1 | 1.89 | 5.36 | - | - | 636 |
| 61 | 7 | 1.51 | 8.23 | 0.58 | 11.27 | 515 |
| 65 | 7 | 1.52 | 7.30 | 0.81 | 10.45 | 675 |
| 69 | 14 | 1.53 | 7.42 | 1.04 | 10.55 | 352 |

(since the distance given by Glass et al. was derived by fitting to the LMC relation). However, the longest period Baade's Window LPVs, which are generally the dusty IRAS sources, lie well

below the LMC relation. Similarly, the LMC OH/IR stars have much longer periods than the optically visible LPVs of similar K magnitude.

In the $(M_{\text{bol}}, \log P)$ diagram, the optically detected LPVs in Baade's Window and the LMC once again lie on the same relation, while most of the Galactic Center LPVs show a lower luminosity, although the offset is smaller than in the $(M_K, \log P)$ diagram. Low M_{bol} values were also found by Jones et al. (1994) and Blommaert et al. (1997) with much smaller samples of stars. At least some of the scatter in the $(M_{\text{bol}}, \log P)$ diagram is due to the scatter in the values of BC_L . This scatter could be reduced by obtaining photometry at wavelengths longer than $3.6 \mu\text{m}$ (L).

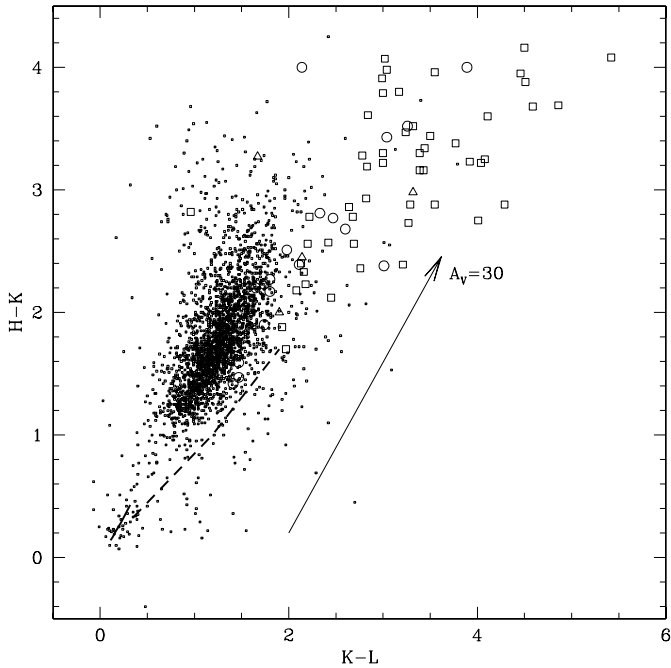


Fig. 6. The composite $(H-K, K-L)$ diagram for variable and non-variable stars in the fields studied. The small points represent the complete set of uncrowded, non-variable objects in all fields, the large open squares are the variable LWHM OH/IR stars, large open triangles are variable Sjouwerman OH/IR stars and large open circles are new variables from Table 3. The short, thick continuous line at the bottom-left represents the unreddened giant branch in Baade’s window while the thick dashed line represents the position of red variables in Baade’s window. The arrow shows the reddening that would result from 30 mag. of visual extinction.

It is usually assumed that low luminosities or, equivalently, very long periods for LPVs are a demonstration of the effect of mass loss on pulsation period. Before the superwind phase of mass loss starts, LPVs of a given metallicity seem to lie on a unique relation as demonstrated by the LMC and Baade’s Window LPVs. Now, for LPVs in general, the pulsation period varies as R^α/M^β , where $\alpha \sim 1.5-2$ and $\beta \sim 0.5-0.9$ depending on whether the LPVs pulsate in the first overtone or fundamental mode (Fox & Wood 1982; Wood 1990). Once the stellar mass has been reduced significantly as a result of a superwind, the pulsation period increases due to the combined effects of the mass reduction and the increase in mean radius that results from structural readjustment (Vassiliadis & Wood 1993). In this situation, the LPVs evolve almost horizontally from their positions as optical variables in the $(M_{\text{bol}}, \log P)$ diagram to the positions found here for the Galactic Center OH/IR stars. This sample of stars is the first to clearly demonstrate this effect over a wide range of luminosities.

The shorter period stars at the top of the envelope of Galactic Center variable stars in Fig. 11, in particular the newly discovered variables, do not have the extremely red intrinsic colours that might be expected if these stars were surrounded by dense circumstellar shells produced by superwind mass loss. The pulsation periods of these stars are probably not greatly affected by

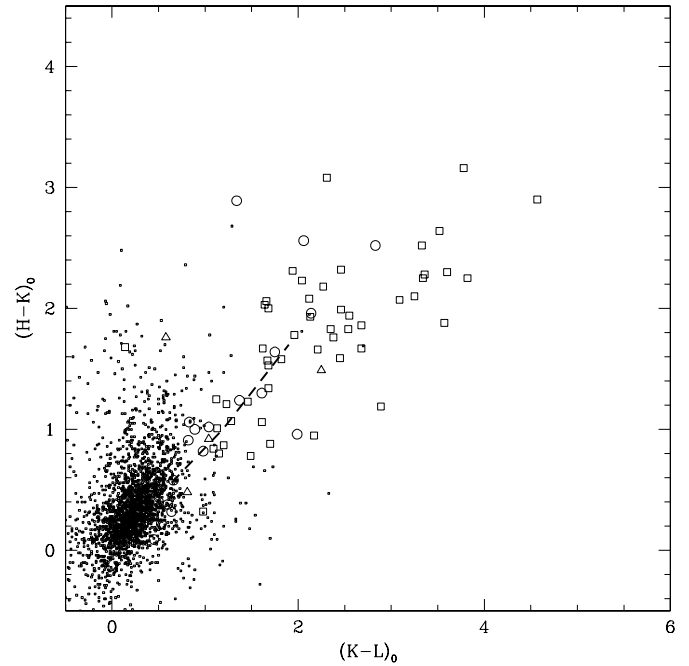


Fig. 7. The stars shown in Fig. 6 after dereddening.

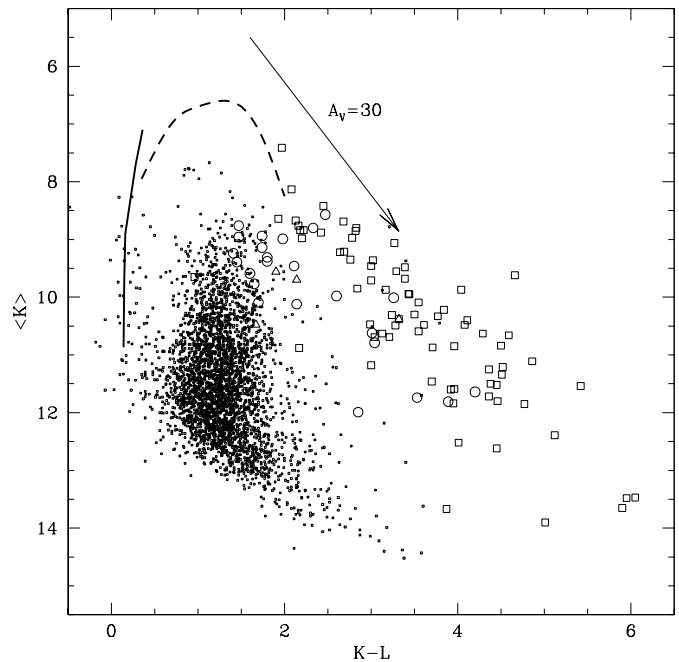


Fig. 8. The composite $(K, K-L)$ diagram for variable and non-variable stars in the fields studied. The symbols and lines are as in Fig. 6.

mass reduction as described above. Such stars with $K-L < 1.3$ are shown in Figs. 10 and 11 as filled symbols (we use this colour cutoff as it corresponds to the red limit of the optically-visible LPVs in Baade’s Window). For $P < 300$ days, these LPVs have M_{bol} and M_K values in excellent agreement with those of LPVs in the LMC and Baade’s Window. The short periods of these stars and the agreement of their luminosities with those of similar LMC LPVs suggest that they are old and of metallicity

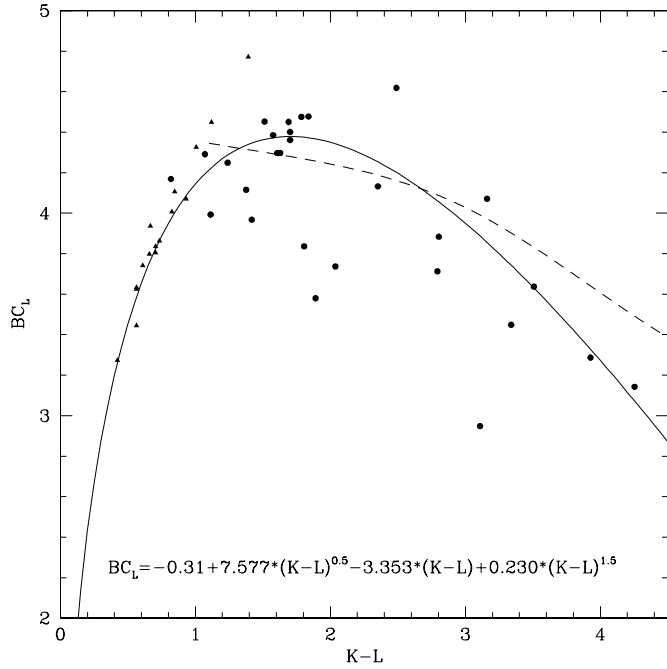


Fig. 9. The bolometric correction to L plotted against $K-L$, where L is defined at $3.59 \mu\text{m}$. The triangles are from data of Wood & Bessell (1983) while the circles are from Whitelock et al. (1991). The continuous line is the fitting formula given on the figure while the dashed line represents the bolometric correction of Blommaert et al. (1997).

up to solar. For example, 47 Tuc with a metal abundance of ~ 0.2 solar has three Miras of period ~ 200 days while the globular clusters NGC5927 and NGC6553, which have near-solar metal abundances and lie in the inner parts of the Galaxy, appear to have Mira variables with periods near 300 days (Andrews et al. 1974). This situation is consistent with solar metallicity being attained in the Galactic Center region during the earliest star formation epoch.

For $P > 300$ days, it is clear that the LPVs without thick dust shells generally fall below the LMC and Baade's Window period-luminosity relations. What we are seeing here is a clear demonstration of the fact that the $(M_{\text{bol}}, \log P)$ and $(M_K, \log P)$ relations for LPVs are metallicity dependent, as predicted by Wood (1990). The long periods in high metallicity LPVs result from the giant branch being redder than for solar metallicity stars. Consequently, the stars will have a larger radius and longer period at a given luminosity. Note, however, that substantial metal abundance variations are required to make the metallicity dependence apparent: Wood (1995) found that the $(M_K, \log P)$ relations for the LMC (metallicity ~ 0.5 solar) and SMC (metallicity ~ 0.25 solar) were consistent with each other.

A rough estimate of the metallicity required to produce the long periods seen for the less extreme stars in Fig. 11 (solid symbols) may be obtained as follows. Wood (1990) found that for LPVs pulsating in the fundamental mode (which we will assume here), $P \propto L^{1.59} Z^{0.46} M^{-1.55}$ (note that this relation was derived for solar metallicity and below, so we will be extrapolating beyond the range of tested parameters here). From

Table 6. Reddening and intrinsic properties of new variables

| LWHM | # | $E(H-K)$ | $\langle K_0 \rangle$ | $(K-L)_0$ | m_{bol} | P |
|------|----|----------|-----------------------|-----------|------------------|------|
| 3 | 7 | 1.70 | 8.10 | - | - | 496 |
| 7 | 10 | 2.05 | 8.69 | 2.06 | 10.97 | 423 |
| 8 | 10 | 1.67 | 9.13 | 0.20 | 11.36 | 316 |
| 13 | 15 | 1.72 | 9.43 | 1.61 | 12.19 | 213 |
| 18 | 18 | 1.38 | 7.92 | 1.61 | 10.69 | 404 |
| 27 | 1 | 1.57 | 7.25 | 0.47 | 10.17 | 305 |
| 34 | 63 | 1.48 | 9.60 | 2.83 | 10.82 | 915 |
| 36 | 3 | 1.15 | 7.05 | 0.64 | 10.13 | 282 |
| 39 | 1 | 1.57 | 7.12 | 0.98 | 10.27 | 355 |
| 41 | 1 | 1.33 | 7.26 | 0.45 | 10.15 | 251 |
| 48 | 3 | 1.36 | 7.35 | 0.82 | 10.51 | 339 |
| 49 | 3 | 1.21 | 7.16 | 0.60 | 10.21 | 256 |
| 51 | 85 | 1.38 | 10.76 | - | - | 769 |
| 60 | 1 | 1.79 | 6.13 | 1.04 | 9.27 | 576 |
| 60 | 29 | 1.79 | 8.12 | 1.75 | 10.75 | 445 |
| 69 | 1 | 1.53 | 6.29 | 1.37 | 9.25 | 858 |
| 70 | 5 | 1.69 | 6.42 | 0.52 | 9.40 | 413 |
| 72 | 2 | 1.68 | 6.64 | 0.53 | 9.63 | 343 |
| 72 | 57 | 1.68 | 9.94 | - | - | 1083 |
| 74 | 2 | 1.51 | 6.74 | 0.89 | 9.90 | 441 |
| 75 | 6 | 1.43 | 7.96 | 0.67 | 11.06 | 470 |
| 78 | 23 | 1.95 | 8.97 | - | - | 390 |
| 92 | 8 | 1.42 | 8.50 | 1.99 | 10.87 | 416 |
| 93 | 31 | 1.44 | 9.49 | 3.16 | 10.18 | 574 |
| 94 | 4 | 1.59 | 6.94 | 0.66 | 10.03 | 339 |
| 103 | 7 | 1.56 | 7.69 | 2.14 | 9.87 | 572 |
| 121 | 6 | 1.14 | 8.07 | 0.83 | 11.23 | 444 |
| 122 | 11 | 1.11 | 8.47 | 1.34 | 11.45 | 657 |
| 126 | 1 | 1.32 | 7.42 | 0.50 | 10.38 | 248 |

Fig. 11, it appears that the bluer Galactic Center stars with $P \gtrsim 300$ days are ~ 0.4 mag. fainter than bulge or LMC stars of the same period. Ignoring any possible difference in mass, we then find from the equation above that we require the Galactic Center metallicity to be ~ 3.6 times higher than the bulge metallicity in order to get the observed offset between the bulge stars and the bluest Galactic Center stars.

Another very important feature of the $(M_{\text{bol}}, \log P)$ diagram is that the luminosities of the main group of Galactic Center OH/IR stars extend considerably brighter than the luminosities of the LPVs in Baade's Window (we exclude the 4 Baade's Window stars that lie above the LMC line in Fig. 11 as they are almost certainly foreground objects). Since final AGB luminosities increase with initial mass (eg. Vassiliadis & Wood 1993) we interpret this to mean that there is a significant component of the intermediate age population of stars near the Galactic Center that does not exist in Baade's Window. If we take $M_{\text{bol}} \sim -6$ as the upper limit to the AGB for the main distribution of Galactic Center LPVs, then Fig. 19 of Vassiliadis & Wood, with an assumed solar metal abundance, indicates a maximum initial mass of $\sim 4 M_{\odot}$ for this group of stars. The empirical calibration of AGB tip luminosities from LMC clusters (Frogel et al. 1990) suggests a similar or greater mass.

As well as the main population of LPVs with $M_{\text{bol}} > -6$, there are several more luminous objects. The presence of

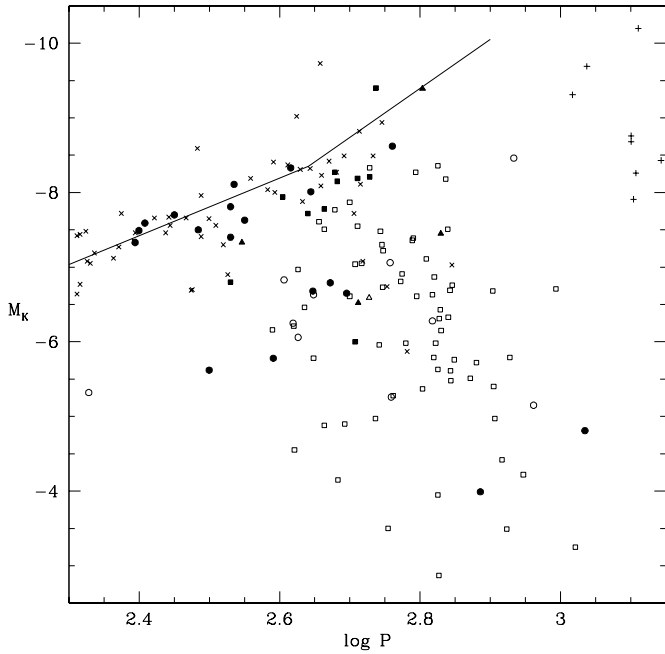


Fig. 10. The $(M_K, \log P)$ diagram for LPVs near the Galactic Center and in Baade's Window and the LMC. The Galactic Center objects are shown as symbols whose shapes have the same meaning as in Fig. 6: the filled symbols are LPVs with $(K-L)_0 < 1.3$. The Baade's Window objects are shown as crosses. The line represents optically visible LPVs in the LMC from Hughes & Wood (1990) while the plus signs represent LMC OH/IR stars from Wood et al. (1992).

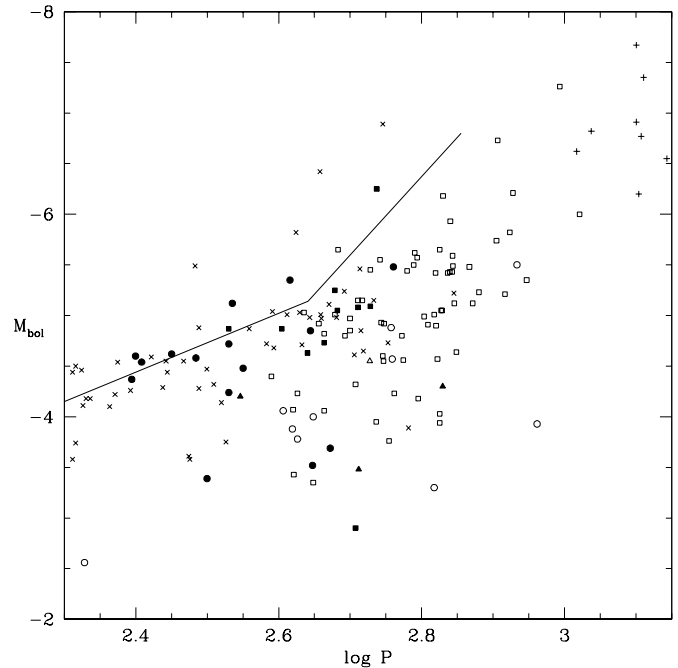


Fig. 11. The $(M_{\text{bol}}, \log P)$ diagram for LPVs near the Galactic Center and in Baade's Window and the LMC. Symbols are as in Fig. 10

stars with an $M_{\text{bol}} < -6$ might be challenged by the suggestion that these are in the foreground and much closer to us than we have assumed. We noted in Sect. 1 that at most a few of the LWHM stars should be foreground objects. The following argument gives strong evidence that at least one of these luminous stars is truly at the centre or beyond. In trying to measure the angular size of the OH masers of several of the LWHM stars, van Langevelde et al. (1992) and Frail et al. (1994) found that the size was unexpectedly large in directions close to the Galactic Center. They concluded that interstellar scattering in the region close the Galactic Center was the most likely cause of the large observed size. One of the sources observed to have a large size was LWHM 33 for which Blommaert et al. (1997) derive $M_{\text{bol}} < -6.2$. In this situation, LWHM 33 must be behind the scattering region and close to the Center and it cannot be a foreground object: its absolute bolometric magnitude is truly < -6.2 . This result supports our conclusion that other LWHM stars have a similar luminosity.

There are two LPVs of long period in our sample (LWHM 28, $P = 806$ days; LWHM 116, $P = 985$) which have $M_{\text{bol}} < -6.5$, consistent with them being young AGB stars with masses $> 6M_{\odot}$ (using the Vassiliadis & Wood results). We also note that the two objects LWHM 70 and 90 are exceptionally red and bright in L although they are relatively faint in K so that periods could not be determined. However, Van Langevelde et al. (1993) determined periods > 1000 days for these two objects (the periods belong to category 2, which are uncertain). Our

photometry suggests that LWHM 70 is not particularly luminous ($M_{\text{bol}} \sim -3.1$) but Blommaert et al. (1997) derive $M_{\text{bol}} = -6$ suggesting this is an AGB star with $M \gtrsim 4M_{\odot}$. LWHM 90 is far too red for our bolometric correction to be applied. If we use our $K - L$ colour and L magnitude with the bolometric correction of Blommaert et al. (1997) for such a red star, we derive $M_{\text{bol}} \sim -7$ as expected for a massive AGB star with $M \sim 6 - 7M_{\odot}$. However, Blommaert et al. (1997) derived a modest luminosity $M_{\text{bol}} = -4.7$. Two other stars with category 2 periods > 1000 days are listed by Van Langevelde et al. (1993). For one of these, LWHM 21, we derive an unambiguous period of 692 days (compared to 1733 derived by Van Langevelde et al.). Blommaert et al. (1997) give a low bolometric luminosity of -3.7 for the other one (LWHM 72). In summary, it appears that there are 2 to 5 massive ($4-7M_{\odot}$) AGB stars currently in the OH/IR phase in the Galactic Center fields studied by LWHM. Since the superwind or OH/IR phase of evolution in stars of $\sim 5M_{\odot}$ lasts about 10^5 years (Vassiliadis & Wood 1993; Tanabé et al. 1997) while the corresponding main-sequence lifetime is $\sim 10^8$ years, there should be about 1000 main-sequence stars of $\sim 5M_{\odot}$ near the Galactic Center for each OH/IR star with initial mass $\sim 5M_{\odot}$. The existence of such stars near the Galactic Center is consistent with a situation where there is ongoing star formation occurring there.

A cautionary note regarding the quantitative estimates of AGB mass is appropriate here. There are no theoretical computations of AGB tip luminosities for stars with metallicity of ~ 3.6 times solar, as estimated above for the Galactic Center LPVs. The results of Vassiliadis & Wood (1993) suggest that AGB tip luminosities for a given initial mass actually reduce with increased metal abundance, which would suggest that the

initial masses derived above for AGB stars are underestimates. However, the theoretical results are highly dependent on the mass loss scheme used and need to be treated with caution. In fact, there are good reasons to believe that the mass estimates of up to $\sim 7M_{\odot}$ given above are too high. Firstly, in the LMC, the OH/IR stars with luminosity near the AGB limit of $M_{\text{bol}} \sim -7$ and probable masses of $5-7M_{\odot}$ attain periods of up to ~ 1500 days (Wood et al. 1992) whereas the maximum period attained near the Galactic Center is ~ 1100 days (see the next section). Secondly, in the plane of our Galaxy, the variable OH/IR stars attain pulsation periods of up to ~ 2800 days (Herman & Habing 1985; Van Langevelde 1990), this period presumably representing the most advanced stage in the evolution of the most massive AGB stars ($M \sim 7M_{\odot}$). Once again the maximum periods in the Galactic Center region are less than in the Galactic plane. Although the maximum mass for the Galactic Center AGB stars remains uncertain, the high luminosities (see above) and long periods (see next section) of these stars leave little doubt that the maximum mass is greater than in the bulge.

7. The period distribution and number densities

The period distribution for the Galactic Center OH/IR stars studied here is shown in Fig. 12. The 1612 MHz maser emission from these stars was found in 6 VLA fields with a total area of ~ 3000 arcmin². In our study of 102 fields, each of size 1 arcmin², we found 29 new LPVs with K amplitudes >0.5 magnitudes, consistent with them being Mira-like, large-amplitude LPVs. To get an estimate of the total number of such LPVs in an area equivalent to that searched for OH/IR stars, we multiply by the area ratio 3000/102. The resultant period distribution for all large amplitude LPVs near the Galactic Center is also shown in Fig. 12. It can be seen that the OH/IR stars are only a small part of the total LPV population.

The OH/IR star population and the complete LPV population near the Galactic Center can now be compared with other populations of LPVs in the Galactic bulge. The population of stars in Baade's window studied by Glass et al. (1995) should be relatively complete as it includes LPVs found in optical and near-infrared (I) surveys as well as IRAS sources. This sample of stars, whose period distribution is also shown in Fig. 12, should be directly comparable to the complete sample of LPVs near the Galactic Center. On the other hand, the sample of bulge IRAS sources studied by Whitelock et al. (1991) should be comparable to the sample consisting of Galactic Center OH/IR stars only, both these samples representing stars in the superwind phase near the end of AGB evolution.

Comparison of the complete samples of LPVs in Baade's Window and at the Galactic Center clearly shows that the LPVs near the Galactic Center attain periods much longer (P up to ~ 1100 days) than the LPVs in Baade's Window (P up to ~ 700 days). This is consistent with the existence of AGB stars near the Galactic Center that are more massive than any existing in Baade's Window. A similar conclusion was derived above based on the luminosities of the longest period objects.

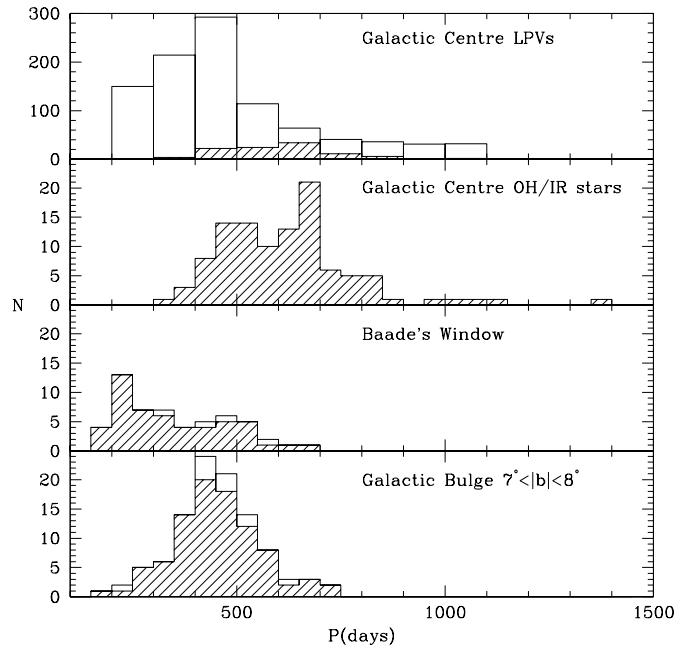


Fig. 12. The period distributions for LPVs near the Galactic Center, in Baade's Window (Glass et al. 1995) and in the Bulge fields studied by Whitelock et al. (1991). In the top panel, the hatched area represents OH/IR stars while the unhatched area represents LPVs detected in this infrared monitoring program but not detected at 1612 MHz. The numbers have been scaled to the area of the 1612 MHz survey. In the bottom two panels, the unhatched areas represent probable foreground objects.

Comparing the Galactic Center OH/IR stars with the bulge IRAS sources, we see once again that the OH/IR stars extend to much longer periods than the bulge sources. As noted above, this can be interpreted as being due to a younger population of AGB stars near the Galactic Center. However, the higher metallicity near the Galactic Center must also contribute to the longer periods observed there.

At the short period end, there are clearly LPVs near the Galactic Center with periods down to 200 days. LPVs with even shorter periods may exist but we did not search for them because of the sparse temporal sampling our data. From Fig. 12 it is clear that there are also many LPVs in Baade's Window with periods down to 200 days. As noted above, the existence of Galactic Centre LPVs with periods near <300 days suggests that an old, metal-poor population exists there.

Glass et al. (1996) have reported preliminary results of a search for LPVs in a $24' \times 24'$ area near the Galactic Center. They found ~ 250 LPVs with K amplitude greater than 0.6 magnitudes in this area, slightly more than the number of LPVs (~ 180) we would predict in a $24' \times 24'$ area from our results. Glass et al. were not able to determine accurate periods for their LPVs, but estimated that about half had $P > 400$ days, while very few had $P < 300$ days. Our results also show that a large fraction of the LPVs have $P > 400$ days. However, unlike Glass et al., we find considerable numbers of LPVs with $P < 300$ days. It will be interesting to see if the large Glass et al. survey

shows substantial numbers of shorter period ($P < 300$ days) LPVs when completed.

8. Wind expansion velocities

The stellar wind expansion velocities v_{exp} obtained from the twin 1612 MHz OH profiles of the Galactic Center OH/IR stars are shown plotted against the pulsation period in Fig. 13. Also shown in the figure are local Mira variables from Sivagnanam et al. (1989) and Dickinson et al. (1975), OH/IR stars within a few degrees of the Galactic plane (the periods come from van Langevelde et al. 1990 and Engels et al. 1983 while the expansion velocities come from Herman & Habing 1985 and Engels et al. 1983), three Galactic bulge variables from the samples of Whitelock et al. (1991) and Glass et al. (1995) for which the Lintel Hekkert et al. (1990) give expansion velocities, and OH/IR stars in the LMC from Wood et al. (1992).

Firstly, we note that the local Miras and bulge stars follow a pattern of increasing v_{exp} with period, starting with $v_{\text{exp}} \sim 3 \text{ km s}^{-1}$ at $\log P = 2.55$ and finishing at $v_{\text{exp}} \sim 17 \text{ km s}^{-1}$ at $\log P = 2.8$. The Galactic plane OH/IR stars tend to have $v_{\text{exp}} \sim 15 \text{ km s}^{-1}$ although these are presumably more massive AGB stars than the local Miras or bulge stars.

The Galactic Center OH/IR stars seem to mirror the sequence of Miras but offset to higher expansion velocities by $\sim 3 \text{ km s}^{-1}$ at a given period. In particular, the mean expansion velocity for $\log P \sim 2.8$ is $\sim 20 \text{ km s}^{-1}$ compared to $\sim 17 \text{ km s}^{-1}$ for the local and bulge Miras.

In order to interpret these results, we make use of the stellar wind models of Habing et al. (1994) which indicate that $v_{\text{exp}} \propto \delta^{0.5} L^{0.3}$, where δ is the dust-to-gas ratio, which we shall assume is proportional to metallicity, and L is the luminosity. An examination of Fig 11 shows that, at a given period, the Galactic Center OH/IR stars are ~ 0.5 mag. less luminous than bulge variables. This is consistent with the results for the 3 bulge OH/IR stars which have a mean $M_{\text{bol}} \sim -5.7$ whereas the equivalent Galactic Center OH/IR stars with $\log P \sim 2.8$ days have $M_{\text{bol}} \sim -5.2$. If we take these luminosities and the respective v_{exp} values of 17 and 20 km s^{-1} , then the formula of Habing et al. (1994) would suggest that the Galactic Center OH/IR stars are ~ 1.6 times more metal rich than the bulge OH/IR stars and local Miras. This is smaller than the factor of ~ 3.6 derived in Sect. 6. However, the two methods of derivation are completely independent.

9. The low and high expansion velocity sources

Lindqvist et al. (1992) examined the spatial and kinematic properties of the LWHM sources and noted that those stars with $v_{\text{exp}} < 18 \text{ km s}^{-1}$ had a larger dispersion in radial velocity and a higher Galactic latitude than the sources with $v_{\text{exp}} > 18 \text{ km s}^{-1}$. This led them to conclude that the OH/IR stars with $v_{\text{exp}} < 18 \text{ km s}^{-1}$ were older than the OH/IR stars with higher v_{exp} .

We now have sufficient data to see if the kinematic and spatial separation into age groups can be seen in the intrinsic

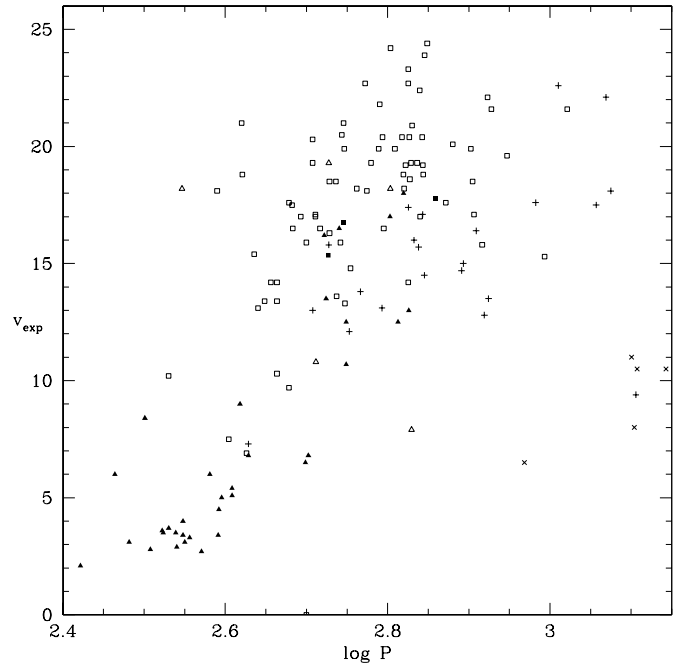


Fig. 13. The stellar wind expansion velocity plotted against period. The expansion velocities for the Galactic Center OH/IR stars are given by LWHM (open squares) and by Sjouwerman (1997) (open triangles). Also shown are local Miras (filled triangles), OH/IR stars near the Galactic plane (plus signs), OH/IR stars in the Galactic bulge (filled squares) and LMC OH/IR stars (crosses). Data sources are given in the text.

properties of the OH/IR stars themselves. In Fig. 14, the Galactic center OH/IR stars are plotted in the $(M_{\text{bol}}, \log P)$ diagram using different symbols to distinguish the stars with $v_{\text{exp}} \geq 18 \text{ km s}^{-1}$ and $v_{\text{exp}} < 18 \text{ km s}^{-1}$. The high and low expansion velocity groups appear to separate into two distinct, parallel sequences. The high expansion velocity stars have longer periods at a given luminosity (by a factor of ~ 1.4) and they generally extend to higher luminosities than the shorter period stars, notable exceptions being the two most luminous, and presumably most massive, objects. Using the relation between period, mass, luminosity and metallicity given in Sect. 6, and assuming the excess period at a given luminosity is due only to a higher metal abundance causing a cooler giant branch, we deduce that the OH/IR stars with higher v_{exp} have ~ 2.1 times the metal abundance of the stars with lower expansion velocity.

The higher luminosities reached by the higher v_{exp} stars almost certainly result from their higher initial mass (younger age), in agreement with the interpretation of the kinematics and spatial distribution of the high and low v_{exp} groups by Lindqvist et al. (1992). The higher mass associated with the high expansion velocity group was ignored in the calculation of the metal enhancement factor given in the previous paragraph. Its inclusion would have required an even greater metal enhancement.

Another interpretation of the separation of high and low expansion velocity objects in Fig. 14 could be as follows. As explained earlier, the OH/IR stars evolve essentially horizontally to longer period in the $(M_{\text{bol}}, \log P)$ diagram. Provided

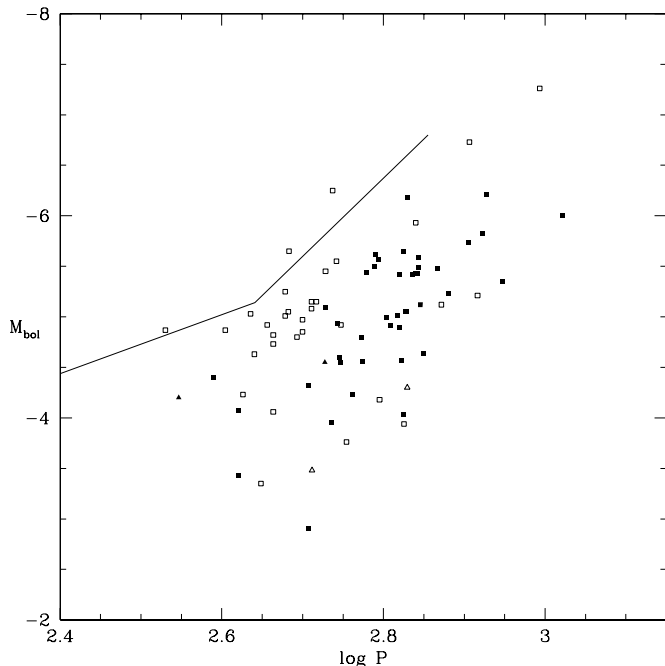


Fig. 14. The $(M_{\text{bol}}, \log P)$ diagram for OH/IR stars near the Galactic Center. Filled symbols represent stars with $v_{\text{exp}} > 18 \text{ km s}^{-1}$ while open symbols represent stars with lower wind expansion velocities. Squares are sources from LWHM and triangles are from Sjouwerman (1997).

v_{exp} increases as the star evolves (perhaps because of the increase in mass loss rate and/or the reduction in stellar mass), the high expansion velocity stars could be explained as more evolved examples of lower expansion velocity stars at the same luminosity. Two difficulties with this picture are (1) there do not seem to be enough low expansion velocity precursors to the highest luminosity examples of the high expansion velocity stars, and (2) we would not expect to see the kinematic differences between the two groups that was noted by Lindqvist et al. (1992). We therefore favour the interpretation of the separation of the two groups given in the previous paragraph.

10. Summary

We have performed infrared monitoring of $102 1' \times 1'$ fields centered on OH/IR stars near the Galactic Center. Periods have been determined for a large number of known OH/IR stars as well as for 29 new large amplitude ($\Delta K > 0.5 \text{ mag.}$) LPVs. We find that the Galactic Center LPV population is dominated by variables that have not been detected as OH masers. The LPVs extend down in period to at least $P \sim 200$ days. Comparison with Mira variables in globular clusters suggests that there are very old stars near the Galactic Center that have sub-solar metallicity. The low luminosities and deduced high metal abundance of nearly all LPVs with $P > 300$ days suggests that solar metallicity was reached at the Galactic Center very early in the life of the Galaxy.

Several pieces of evidence suggest that there are intermediate age AGB stars near the Galactic Center. Firstly, the luminosities

of the Galactic Center LPVs extend to higher values than in Baade's Window or in the bulge at $7^\circ < |b| < 8^\circ$. Secondly, the maximum periods attained by the Galactic Center OH/IR stars are > 1000 days whereas LPVs in the bulge all have periods < 750 days. Comparison of luminosities and periods with theoretical models of AGB evolution suggest that a significant component of the intermediate age population could be as massive as $\sim 4M_\odot$ with a few stars extending in mass to $\sim 7M_\odot$. There should be approximately 1000 times as many main-sequence stars of similar mass in the same volume of space. However, these estimates must remain very uncertain as the Galactic Center stars are almost certainly very metal rich and no theoretical AGB calculations covering the required metallicity range exist.

There are a number of pieces of evidence suggesting that the stars near the Galactic Center have metallicities $\sim 2\text{--}4$ times solar, and that the metal abundance has increased with time there. Firstly, in the $(M_{\text{bol}}, \log P)$ diagram, there is a general offset of the sequence of Galactic Center LPVs with $P > 300$ days from the equivalent sequences of LPVs in the Galactic bulge and the LMC, the offset being in the sense of causing longer periods at a given luminosity. The offset has been interpreted as due to high metallicity in the Galactic Center stars causing a lower T_{eff} on the AGB and hence larger radii and longer pulsation periods at a given luminosity. The results clearly demonstrate that the $(M_{\text{bol}}, \log P)$ and $(M_K, \log P)$ relations are metallicity dependent.

Galactic Center LPVs with stellar wind expansion velocities $\geq 18 \text{ km s}^{-1}$ and $< 18 \text{ km s}^{-1}$ fall into two distinct sequences in the $(M_{\text{bol}}, \log P)$ diagram. Stars in the lower expansion velocity group have shorter periods at a given luminosity than stars in the higher expansion velocity group, a results that can be explained by the longer period stars having a metallicity > 2 times that of the shorter period stars. The higher expansion velocity group extends to higher luminosities than the lower expansion velocity group, suggesting that the stars of higher v_{exp} are younger. This result agrees with studies of the kinematics and spatial distribution of the OH/IR stars. The combination of the above results points to continuing metal richment and star formation near the Galactic Center.

References

- Andrews P.J., Feast M.W., Lloyd Evans T., Thackeray A.D., Menzies J.W., 1974, *Observatory* 94, 133
- Allen D.A., 1994, in *The Nuclei of Normal Galaxies: Lessons from the Galactic Center*, NATO Advanced Research Workshop, eds. R. Genzel & A.I. Harris (Kluwer), p.293
- Baud B., Habing H.J., Matthews H.E., O'Sullivan J.D., Winnberg A., 1975, *Nature* 258, 406
- Bessell M.S., Brett J.M., 1988, *PASP* 100, 1134
- Blommaert J.A.D.L., van der Veen W.E.C.J., Habing H.J., 1993, *A&A* 267, 39
- Blommaert J.A.D.L., van der Veen W.E.C.J., Van Langevelde H.J., Habing H.J., Sjouwerman L.O. 1997, *A&A*, in press
- Cotera A.S., Erickson E.F., Colgan S.W.J., Simpson J.P., Allen D.A., Burton M.G., 1996, *ApJ* 461, 750
- Dickinson D.F., Kollberg E., Yngvevsson S., 1975, *ApJ* 199, 131

- Engels D., 1982, PhD Thesis, Bonn
- Engels D., Kreysa E., Schultz G.V., Sherwood W.A., 1983, *A&A* 124, 123
- Feast M.W., Glass I.S., Whitelock P.A., Catchpole R.M., 1989, *MNRAS* 241, 375
- Frogel J.A., Whitford A.E., 1987, *ApJ* 320, 199
- Frogel J.A., Mould J.R., Blanco V.M., 1990, *ApJ*, 352, 96
- Fox M.W., Wood P.R., 1982, *ApJ* 259, 198
- Frail D.A., Diamond P.J., Cordes J.M., Van Langevelde H.J., 1994, *ApJL* 427, 43
- Glass I.S., Whitelock P.A., Catchpole R.M., Feast M.W., 1995, *MNRAS* 273, 383
- Glass I.S., Matsumoto S., Ono T., Sekiguchi K., 1996, in Proc. 4th ESO/CTIO Workshop, The Galactic Center, ed. R. Gredel, ASP Conf. Ser. 102, 312
- Habing H.J., Tignon J., Tielens A.G.G.M., 1999, *A&A* 286, 523
- Harvey P.M., Bechis K.P., Wilson W.J., Ball J.S., 1974, *ApJS* 27, 331
- Herman, J., Habing H.J., 1985, *A&AS* 59, 523
- Hughes S.M.G., Wood P.R., 1990, *AJ* 99, 784
- Jones T.J., McGregor P., Gehrz R.D., Lawrence G.F. 1994, *AJ* 107, 1111
- Krabbe A., Genzel R., Eckart A., Najarro F., Lutz D., Cameron M., Kroker H., Tacconi-Garman L.E., Thatte N., Weitzel L., Drapatz S., Geballe T., Sternberg A., Kudritzki R., 1995, *ApJL* 447, L95
- Le Bertre T., 1993, *A&AS* 97, 729
- Le Sidenar P., Le Bertre T., 1993, *A&A* 278, 167
- Le Sidenar P., Le Bertre T., 1996, *A&A* 314, 896
- Lindqvist M., Habing H.J., Winnberg A., 1992, *A&A* 259, 118
- Lindqvist M., Winnberg A., Habing H.J., Matthews H.E., 1992, *A&AS* 92, 43
- McGregor P., 1994, Mount Stromlo & Siding Spring Observatories document, <http://msowww.anu.edu.au/observing/docs/manual/manual.html>
- McGregor P., Hart J., Hoadley D., Bloxham G., 1994, in *Infrared Astronomy with Arrays*, ed. I. McLean (Kluwer), p.299
- Rieke G.H., Lebofsky M.J., 1985, *ApJ* 288, 618
- Schechter P.L., Mateo M., Saha A., 1993, *PASP* 105, 1342
- Sivagnanam P., Le Squeren A.M., Foy F., Tran Minh F. 1989, *A&A* 211, 341
- Sjouwerman L.O., 1997, PhD Thesis, Chalmers University of Technology
- Stellingwerf R.F., 1978, *ApJ*, 224, 953
- Tanabé T., Nishida S., Matsumoto S., Onaka T., Nakada Y., Soyano T., Ono T., Sekiguchi K., Glass I.S., 1997, *Nature* 385, 509
- te Lintel Hekkert P., Caswell J.L., Habing H.J., Haynes R.F., Norris R.P., 1990, *A&AS* 90, 327
- Van Langevelde H.J., Frail D.A., Cordes J.M., Diamond P.J., 1992, *ApJ* 396, 686
- Van Langevelde H.J., van der Heiden, R., van Schooneveld, C., 1990, *A&A* 239, 193
- Van Langevelde H.J., Janssens A.M., Goss W.M., Habing H.J., Winnberg A., 1993, *A&AS* 101, 109
- Vassiliadis E., Wood P.R., 1993, *ApJ* 413, 641
- Whitelock P., Feast M., Catchpole R., 1991, *MNRAS* 248, 276
- Wood P.R., 1990, in *From Miras to Planetary Nebulae: Which Path for Stellar Evolution?*, eds. M.O. Mennessier & A. Omont (Yvette Cedex: Editions Frontieres), 67
- Wood P.R., 1995, in *Astrophysical Applications of Stellar pulsation*, eds. R.S. Stobie & P.A. Whitelock, ASP Conf. Series 83, 127
- Wood P.R., Bessell M.S. 1983, *ApJ* 265, 748
- Wood P.R., Whiteoak J.B., Hughes S.M.G., Bessell M.S., Gardner F.F., Hyland A.R., 1992, *ApJ* 397, 552